Investigation of structural, optical, electrical, and optoelectronic properties of Co-doped ZnO thin films

NESLIHAN UZAR[1,2,*], UBADE ABDULAZIZ[3]
[1]*Department of Physics, Science Faculty, Istanbul University, Vezneciler, 34134 Istanbul, Turkey*
[2]*Nanomaterial Characterization and Device Design Lab, Department of Physics, Science Faculty, Istanbul University, Vezneciler, 34134 Istanbul, Turkey*
[3]*Institute of Science, Istanbul University, Suleymaniye, Istanbul, Turkey*

In this study, undoped ZnO and cobalt (Co)-doped ZnO thin films with varying Co dopant concentrations ($Zn_{1-x}Co_xO$, x=0.01, 0.02, 0.03, and 0.05) were successfully fabricated on the glass and p-type silisyum (Si) substrates using the sol-gel dip coating and spraying methods. All thin films were found to be pure and exhibited a wurtzite ZnO polycrystalline structure with a preferred orientation along the (002) plane. The produced thin films exhibited nanofiber surface morphologies composed of nanodots. It was observed that the surface homogeneity of the thin films improved with Co doping, with the most favorable outcome observed in the 1% Co-doped ZnO sample. Additionally, it was noted that the crystal size of ZnO decreased with Co doping from 25 nm to 14 nm. At low cobalt doping ratios, no significant changes were observed in the optical transmittance and band gap energy of ZnO. However, with higher doping amount (5% Co doping), a decrease in optical transmittance from 70% to 55% and a reduction in the band gap energy from 3.22 eV to 3.05 eV were observed. For low doping rates, no significant change in the electrical properties of ZnO thin films was observed; however, with 5% Co doping, the resistance value of the ZnO thin film increased from $2.3x10^4$ Ω to $4.0x10^6$ Ω, accompanied by a decrease in leakage current from $1.9x10^{-6}$ A to $3.8x10^{-9}$ A. Finally, the efficiencies of the obtained thin films as solar cells and photodiodes were investigated under both dark and light conditions of 100 mW/cm^2. It was observed that Co doping decreased the performance of ZnO as a solar cell. However, it was found that the produced Au/ $Zn_{0.99}Co_{0.01}O$/p-Si diode was highly suitable for use as a photodiode for visible light sensor applications, with a photosensitivity value of $1.27x10^{-1}AW^{-1}$, while pure ZnO is active in the UV region. Since the structural and photodiode properties of ZnO were enhanced by 1% Co doping, this sample held promise for optoelectronic devices.

(Received September 25, 2023; accepted July 30, 2024)

Keywords: Co-doped ZnO, Photovoltaic cell, Photodiode, SEM, EDS, XRD

1. Introduction

Today, as technology develops rapidly to meet the needs of humanity, there is a growing demand for energy and new devices. The gradual decline in fossil resources, which currently fulfill the majority of the world's energy requirements, is heightening interest in renewable energy. Among renewable energy sources, the sun is the most abundant, clean, environmentally friendly and locally available. Electricity production from the sun is provided through solar cells (photovoltaic cells). Silicon semiconductor element is predominantly utilized in both solar cells and various technological devices. However, the search for new materials has commenced due to the depletion of silicon reserves and the escalation of its prices. Among these elements, ZnO is highly favored due to its wide band gap (3.37 eV), large binding energy (60 meV), high transmittance in the visible light spectrum, chemical stability, non-toxic nature, and cost-effective production. Thanks to these features, ZnO has many application areas such as solar cell, LED, gas sensor, piezoelectric transducers, solar energy storage, and photodetector [1-12]. ZnO holds significant importance, especially for optoelectronic devices, due to its transparent conductive structure [13]. Furthermore, when ZnO is doped with transition metals, the defects formed within the structure alter the material's energy levels and surface states, enabling improvements in ZnO's structural, optical, and electrical properties [14].

Previous studies have demonstrated that cobalt, as one of the transition elements, exerts a significant influence on the magnetic and optical properties of ZnO. Particularly, the capability to modify the material's band gap to enhance light absorption properties holds great importance in enhancing the performance of various optoelectronic devices, such as solar cells and photodetectors [14]. Additionally, since Co (58 pm) and Zn (60 pm) have similar ionic radii, Co doping does not cause a significant change and/or distortion in the crystal structure of ZnO. Although numerous studies have been conducted on the production of Co-doped ZnO and their application in magnetoelectronic and spintronic devices [15-18], their potential in optoelectronic applications, such as solar cells and photosensors, has been limitedly investigated [3,19]. In recent studies in the field of photovoltaics, Co-doped ZnO thin film was used as an electron transport layer for perovskite solar cell, and the efficiency of the solar cell was found to be 7% [20]. In the study conducted by G.

Kanimozhi et al., Co-doped ZnO was utilized as a photoanode for dye-sensitized solar cells. It was observed that the solar cell efficiency increased compared to the use of pure ZnO, reaching 1.63% [21]. In other studies, Co-doped ZnO material was employed as an antireflective coating for silicon solar cells, effectively enhancing the performance of the solar cells [22]. As a photosensor, the response of the material to UV light was generally examined. These studies demonstrated that the sensitivity to UV light of Co-doped ZnO was high, especially for 1% Co-doped ZnO [23]. So far, conventional form solar cells (n-p junction) with Co-doped ZnO have not been extensively studied. Only in one article in the literature, the photovoltaic properties of the structure coated with Co-doped ZnO on n-type Si were determined by short circuit current (I_{SC}) and open circuit voltage (V_{OC}). Additionally, in this study, it was roughly shown that the diode structure acted as a phodiode type sensor against visible light [3]. It is evident that there are not enough studies in the field of optoelectronics of Co-doped ZnO thin film, especially for visible light spectrum. In this study, the primary aim is to determine the changes in the optoelectronic properties of pristine ZnO thin film when cobalt is doped into ZnO. Many methods such as metal organic chemical vapor deposition (MOCVD), molecular beam epitaxy (MBE), pulsed laser deposition, and sol-gel are utilized to produce doped ZnO samples [24-28]. Among these methods, the sol-gel method stands out due to its low cost, ease of use, and wide application area [29]. If the sol-gel method is employed to synthesize nanostructured semiconductor materials, additional techniques such as dip coating, spin coating, and spraying methods are required to form thin films.

In this study, ZnO thin films doped with various mole ratios of Co ($Zn_{1-x}Co_xO$, x=0.0, 0.01, 0.02, 0.03, and 0.05) were produced on glass and p-type Si substrates using the sol-gel dip coating and spraying methods. After production, the structural, optical, electrical, and optoelectronic properties of these thin films were examined and compared to undoped ZnO. At the end of the present study, it was determined whether Co-doped ZnO thin films could be used as an optoelectronic device such as a solar cell or photodiode. Thus, some light was shed on this under-researched subject.

2. Experimental

2.1. Synthesis of $Zn_{1-x}Co_xO$ (x=0.0, 0.01, 0.02, 0.03, and 0.05) solutions by the sol-gel method

$Zn_{1-x}Co_xO$ (x=0.0, 0.01, 0.02, 0.03, and 0.05) solutions were synthesized using the sol-gel method to produce thin films on glass and Si substrates. Zinc acetate dihydrate ($(CH_3COO)_2Zn.2H_2O$) and cobalt (II) acetate tetrahydrate ($Co(CH_3COO)_2{\cdot}4\ H_2O$) were utilized as zinc and cobalt source material, respectively. The molarity of each solution was determined as 0.5. After calculating the amounts of the source materials depending on their mole ratio in the solution, the source materials were weighed using a precision balance. The weighed source materials were dissolved in ethylene glycol monomethyl ether ($C_3H_8O_2$), serving as the solvent, using a magnetic stirrer operating at a speed of 800 rpm. After approximately 30 minutes of stirring to ensure homogeneity, ethanolamine (C_2H_7NO) was added as a catalyst to the five prepared solutions. The molar ratio of ethanolamine to zinc is typically maintained at "1". Following the addition of the catalyst to the solutions, stirring continued for two hours. Throughout the mixing process, the temperature of the solutions was maintained constant at 65°C.

2.2. Preparation of $Zn_{1-x}Co_xO$ (x=0, 0.01, 0.02, 0.03 and 0.05) thin films

The thin film coating process began with the cleaning of p-type Si and glass substrates intended for use as coating substrates. While glass substrates were utilized for structural and optical analyses, p-type Si substrates were employed for electrical and optoelectrical measurements. Initially, glass and p-type Si substrates were boiled in technical acetone for a period of time. Subsequently, glass substrates were sequentially immersed in ethanol and a mixture composed of 3 units HCl and 1 unit HNO_3, and left to stand for approximately 10 minutes. The Si substrates were boiled in a solution consisting of 1 unit NH_3, 1 unit H_2O_2, and 4 units distilled water at 150°C for 15 minutes to remove contaminants. In the final step of the cleaning process, p-type Si substrates were etched in hydrofluoric acid (HF) for 5-10 seconds to remove the oxide layer from the surface [30]. Between all stages of the cleaning process, both glass and p-type Si subtrates were rinsed with deionized water. After the cleaning process, Co-doped and undoped ZnO solutions were coated on glass substrates via the dip coating method for structural and optical analyses. The coating process was repeated 15 times for structural analysis and 6 times for optical analysis. All ZnO solutions were deposited onto p-type Si substrates in 6 layers by spraying method for use in optoelectronic and electrical measurements. After each coating process, each sample was subjected to a pre-annealing process at 320°C for 2 minutes to eliminate unwanted chemical solvents and organic residues. Finally, the produced all thin films were annealed for 30 minutes in a box oven at 500^0 C to complete the formation of the crystal structure of samples. In this paper, undoped ZnO, ZnO films doped with 1% Co, 2% Co, 3% Co, and 5% Co are referred to as Z, C1, C2, C3, and C5, respectively.

After the production stage of thin films was completed, gold (Au) contacts were thermally deposited on the back and front parts of the $Zn_{1-x}Co_xO$/p-type Si diodes using NANOVAK-NVTH-350 apparatus. The front electrodes were created in the form of dot with a diameter of 1 mm and a thickness of 200 nm. Figs. 1(a) and (b) depict the actual image and schematic representation of the Au/$Zn_{1-x}Co_xO$/p-type Si/Au structures, respectively.

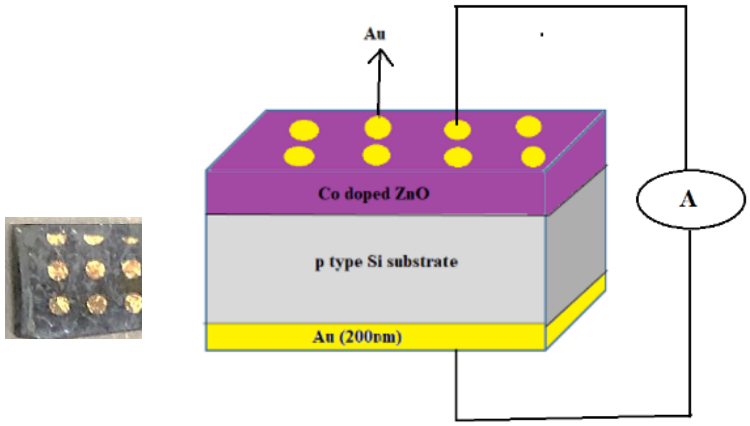

Fig. 1. (a) Actual image and (b) Schematic representation of the Au/$Zn_{1-x}Co_xO$/p-type Si/Au diodes (color online)

2.3. Characterization methods for $Zn_{1-x}Co_xO$ (x=0.0, 0.01, 0.02, 0.03, and 0.05) thin films properties

The crystal structures of thin films deposited on glass substrates with various Co mole ratios were determined via XRD analysis (CuKα radiation with 1.54060 Å) in the range of 25° to 80° with a step size of 0.0130 using the APD 2000 PRO XRD system. The particle sizes with surface morphologies, and chemical compositions of all thin films were examined via SEM and EDS analyses, respectively, with a Zeiss-EVOLS 10 device. The optical properties of all samples were measured through optical transmittance analysis in the range of 200-1100 nm under ambient air conditions at room temperature using a PERKIN ELMER UV-VIS spectrometer. The optoelectronic properties of the thin films were tested using the ORIEL Sol 1A solar simulator with an illumination intensity of 100 mW/cm^2. All electrical measurements of the thin films were conducted using a Keithley 2400 multimeter.

3. Results and discussion

Fig. 2 illustrates the surface morphologies of $Zn_{1-x}Co_xO$ (x = 0.0, 0.01, 0.02, 0.03, and 0.05) thin films deposited on glass substrates. It can be observed from Fig. 2 that the surface of the thin films is composed of nanofibers, as shown at a magnification of 5,000x.The Z sample exhibits the most irregular and non-homogeneous surface morphology among the thin films. However, it is evident that the C1 thin film possesses the most homogeneous and smooth surface. It is understood that thin films with different Co doping ratios shown in Figs. 2 (b-e) display a smoother nanofiber structure than that of pure ZnO. Similar SEM images revealing a nanofiber structure were observed in other studies involving Co doping [3].

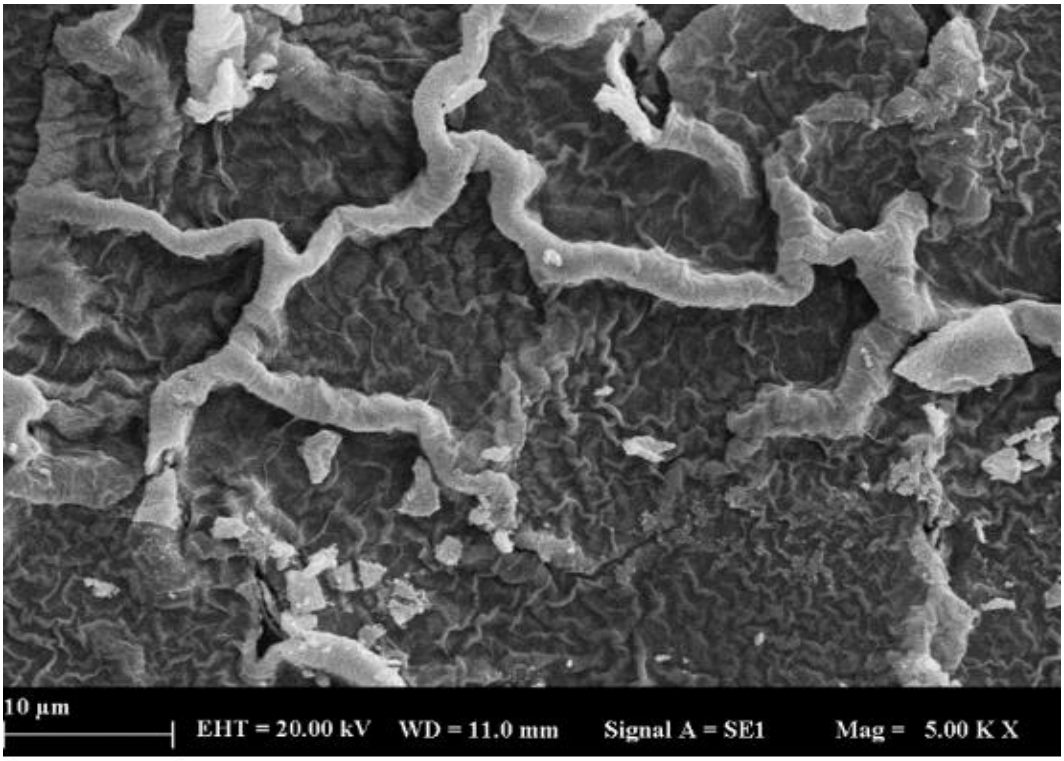
10 µm
EHT = 20.00 kV WD = 11.0 mm Signal A = SE1 Mag = 5.00 K X

(a)

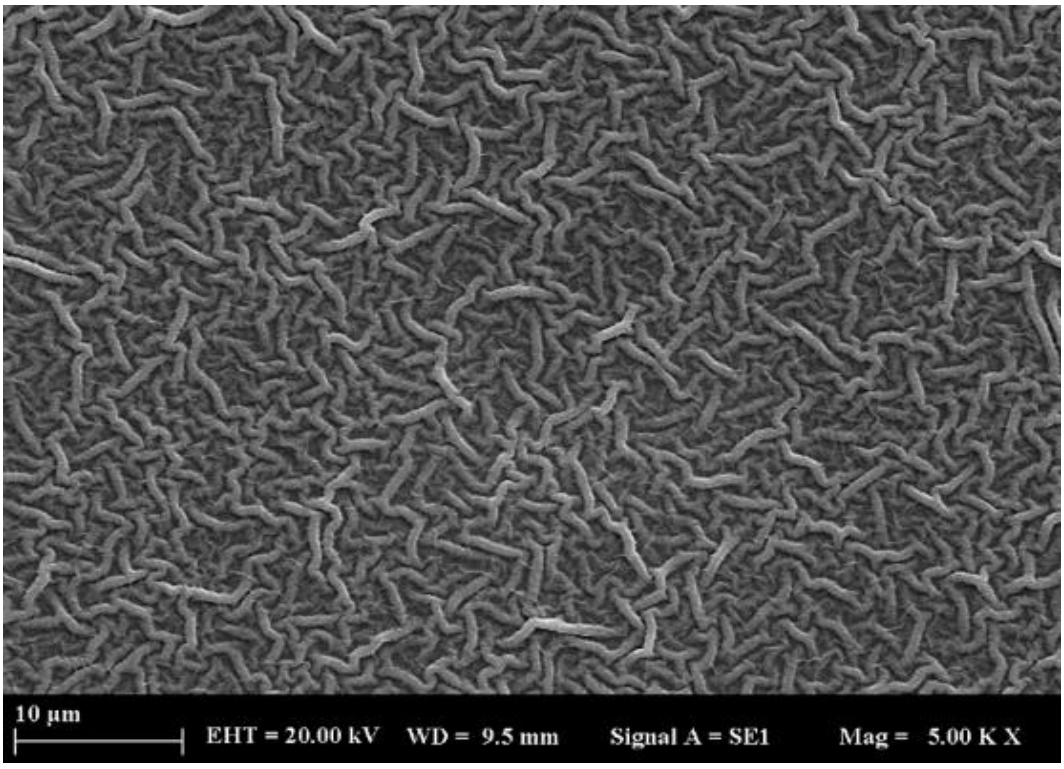
10 µm
EHT = 20.00 kV WD = 9.5 mm Signal A = SE1 Mag = 5.00 K X

(b)

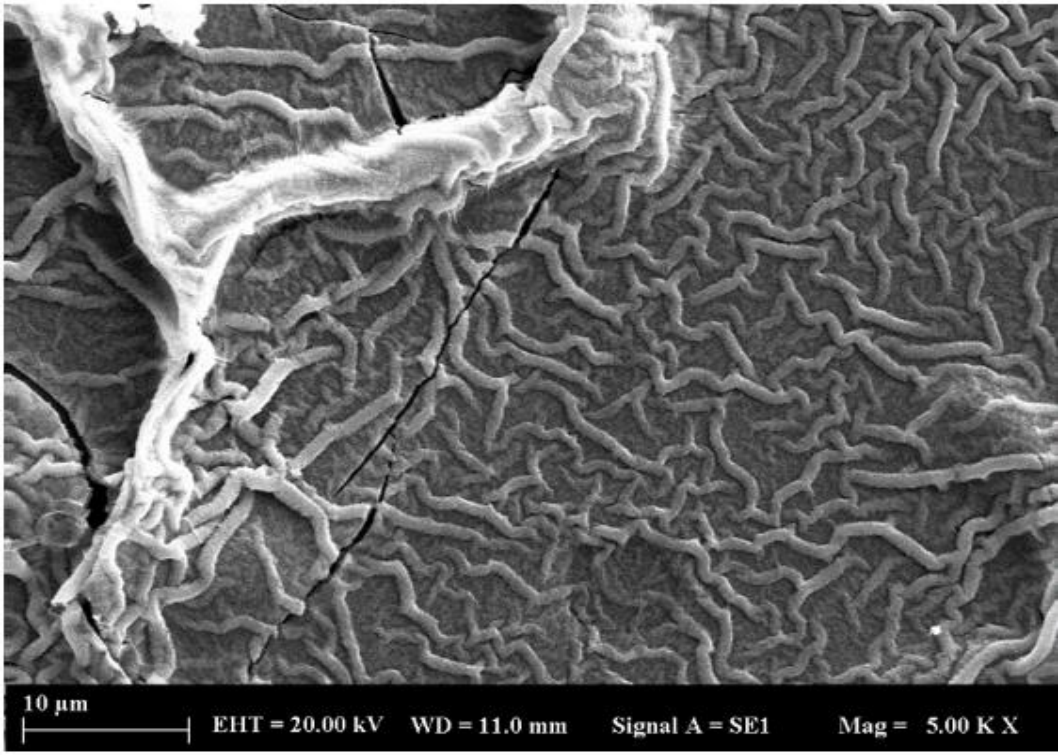
10 µm
EHT = 20.00 kV
WD = 11.0 mm
Signal A = SE1
Mag = 5.00 K X

(c)

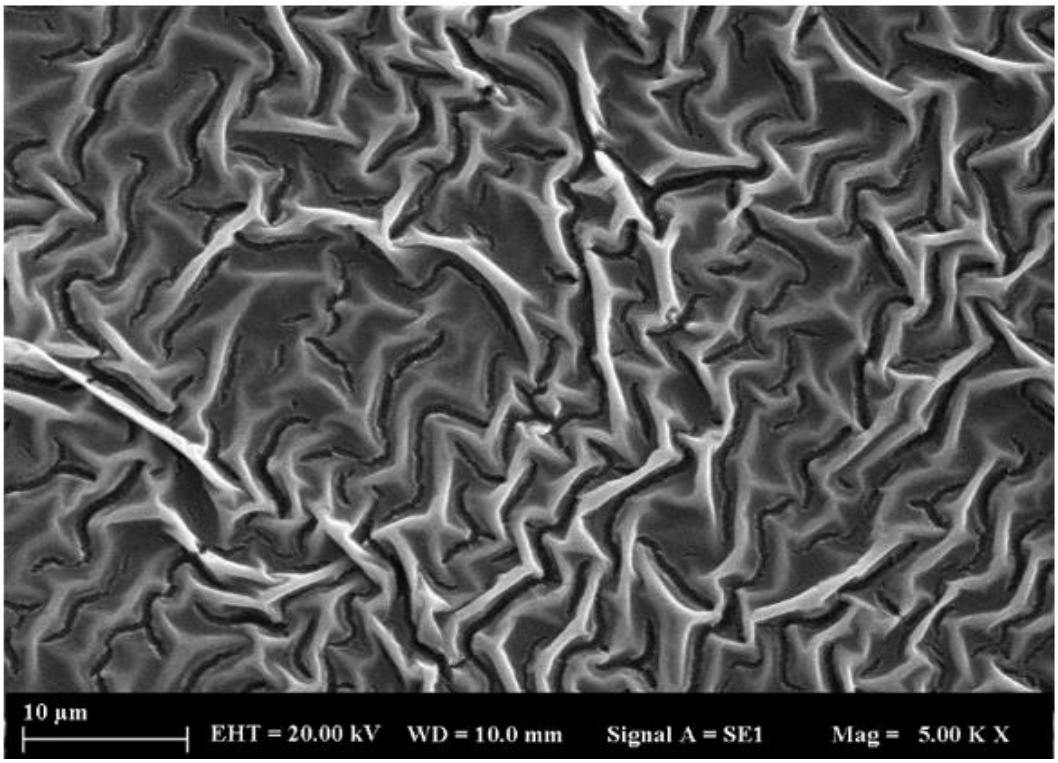
10 µm
EHT = 20.00 kV
WD = 10.0 mm
Signal A = SE1
Mag = 5.00 K X

(d)

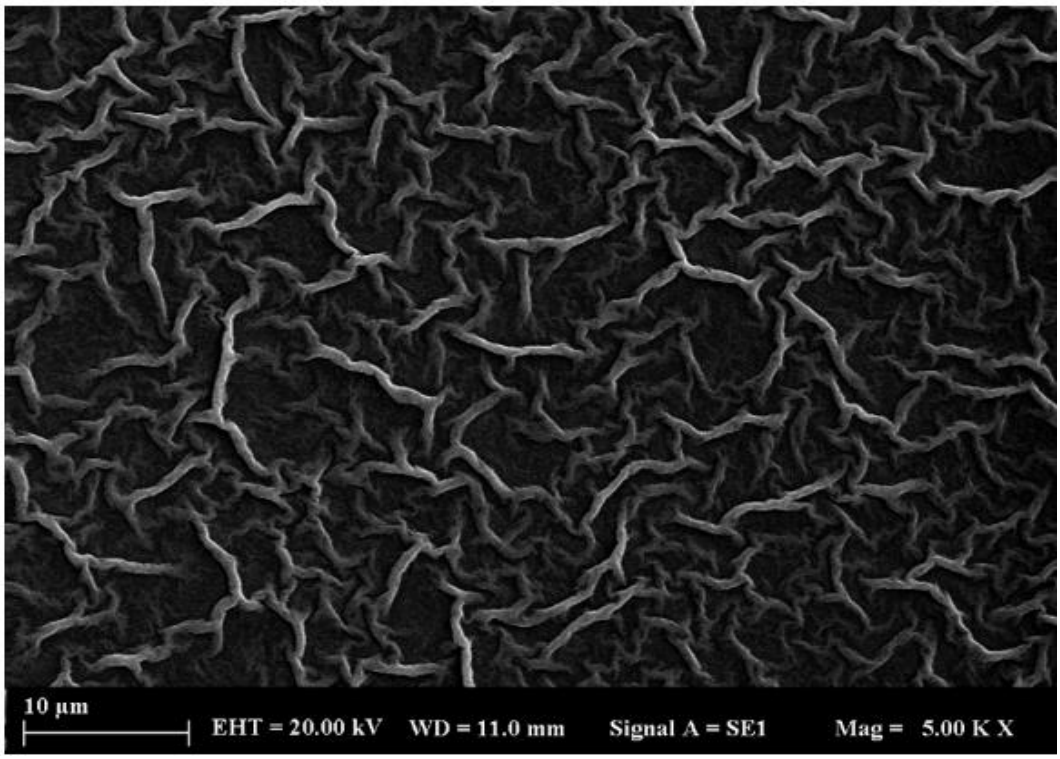

(e)

Fig. 2. SEM images of a) Z, b) C1, c) C2, d) C3, and e) C5 thin films with 5000x magnification

When SEM images are examined at 100,000x magnification, it becomes apparent that nanofibers actually form through the merging of nanodots (Figs. 3 (a-e)). It is observed from Fig. 3 (a) that the diameters of the nanodots belonging to the undoped ZnO sample are in the range of 50-70 nm. From Fig. 3(b), the diameter of nanodots in the C1 sample varies between 35 and 45 nm. The average particle size of nanodots for the C2 sample is found to be in the range of 35-40 nm (Fig. 3 (c)). According to the SEM image shown in Fig. 3(d), it is observed that the nanodots on the surface of the C3 thin film are clustered together quite densely. The particle size of the C3 thin film is nearly 35-40 nm on average. Nanodots with diameters ranging from 25 to 35 nm are observed to be formed, as indicated by the SEM image of 5% Co-doped ZnO, shown in Fig. 3 (e). These results indicate that Co doping affects the morphology of pristine ZnO, and it is understood that the average particle size decreases slightly as the doping concentration increases. Co doping may alter the nucleation rate of ZnO nanoparticles, leading to the formation of smaller nuclei and subsequently smaller particles [31].

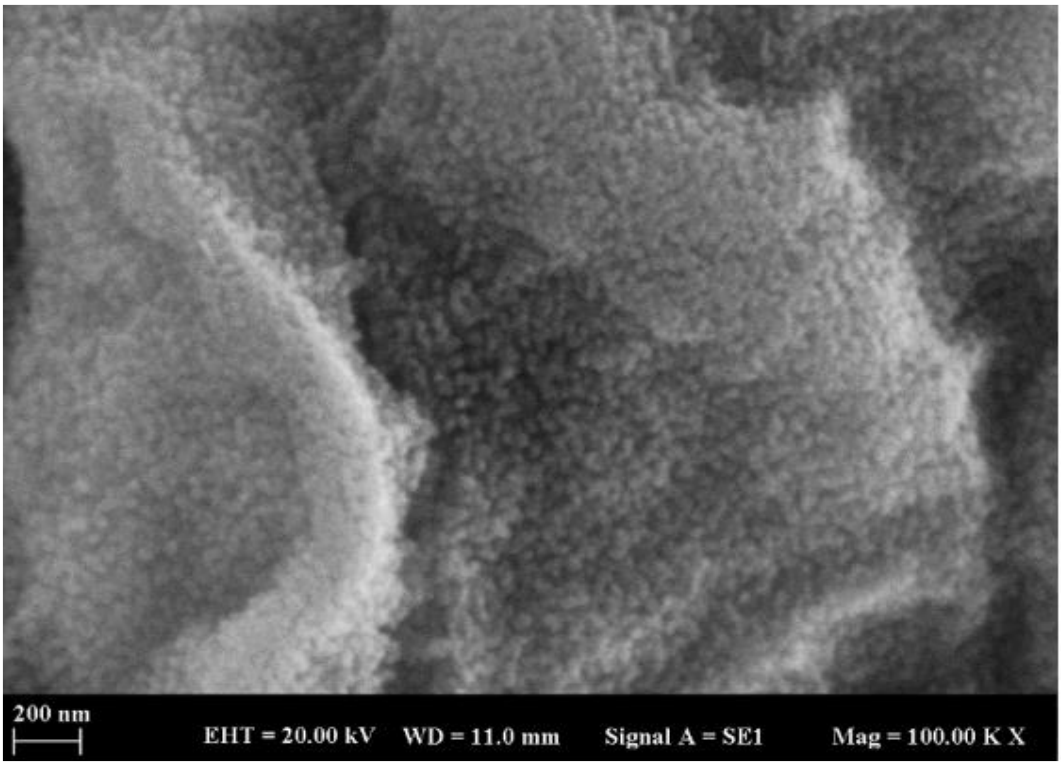
200 nm
EHT = 20.00 kV
WD = 11.0 mm
Signal A = SE1
Mag = 100.00 K X

(a)

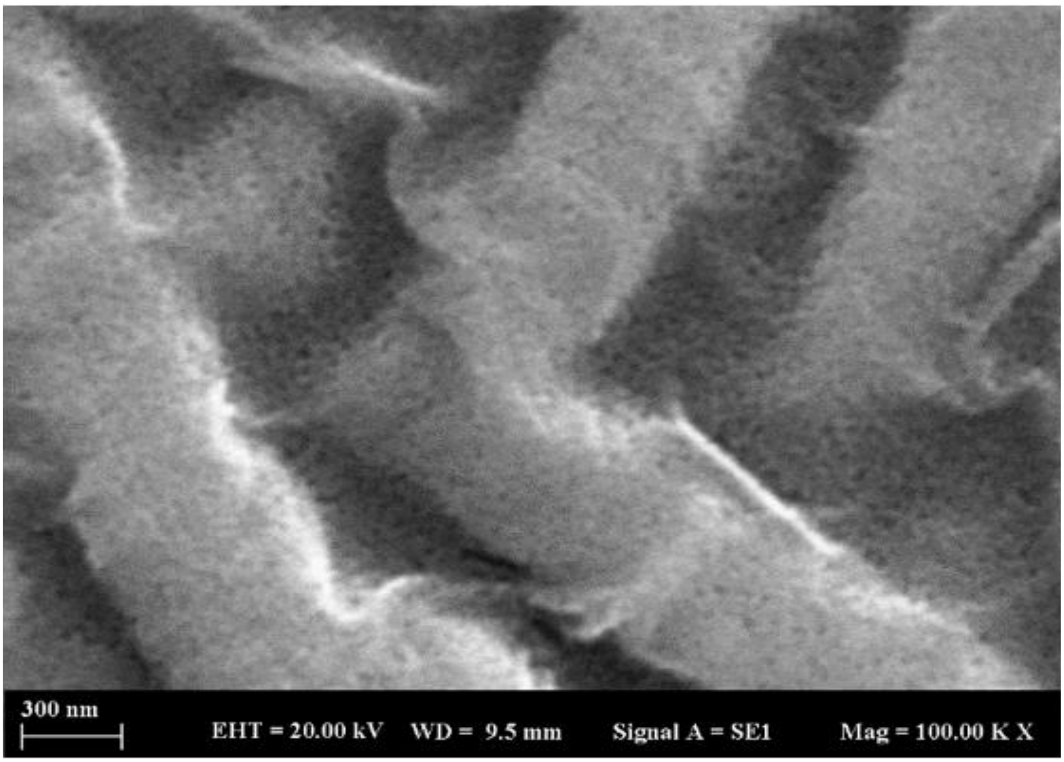
300 nm
EHT = 20.00 kV
WD = 9.5 mm
Signal A = SE1
Mag = 100.00 K X

(b)

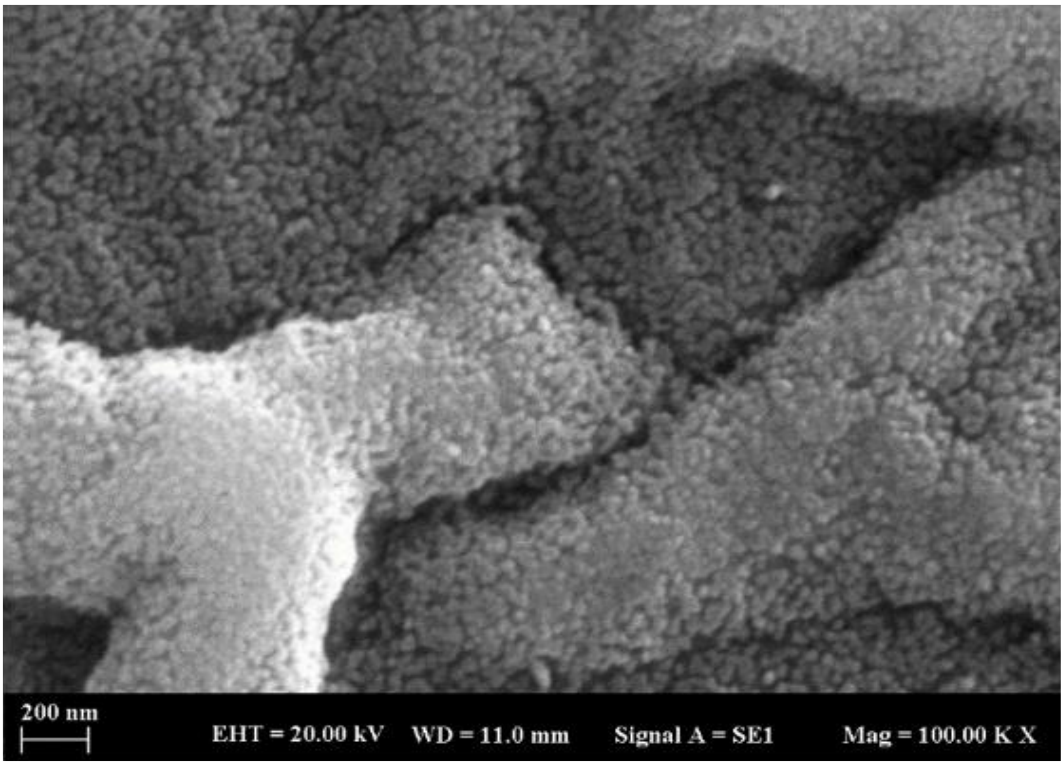
200 nm
EHT = 20.00 kV
WD = 11.0 mm
Signal A = SE1
Mag = 100.00 K X

(c)

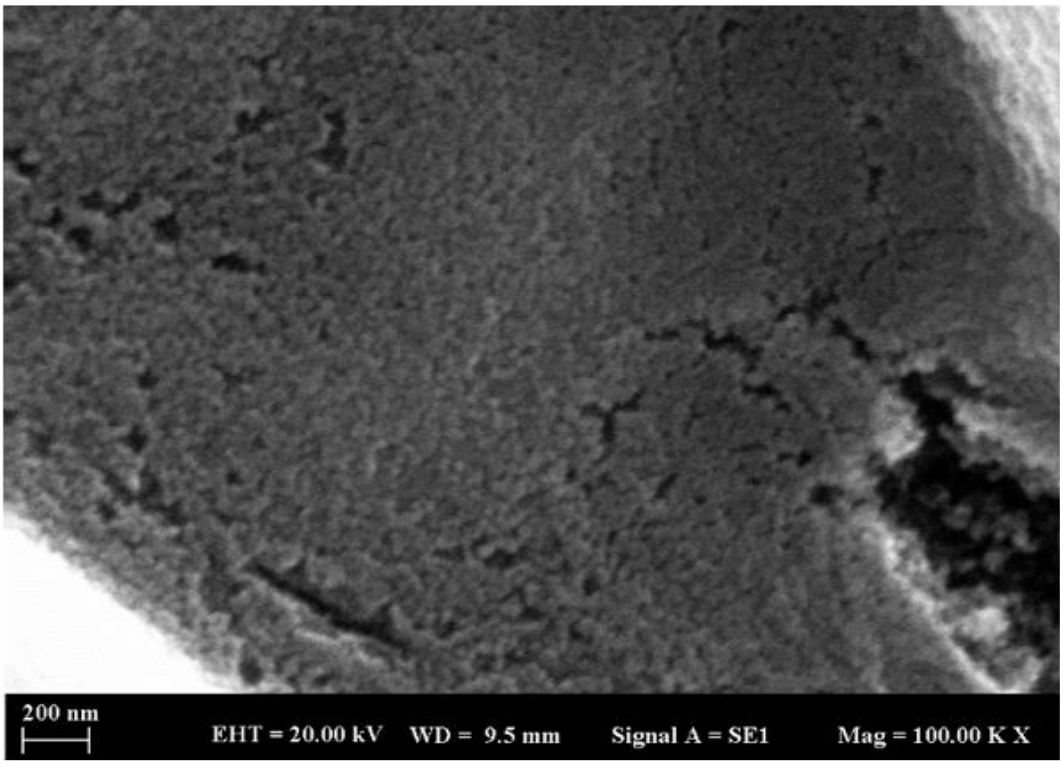
200 nm
EHT = 20.00 kV
WD = 9.5 mm
Signal A = SE1
Mag = 100.00 K X

(d)

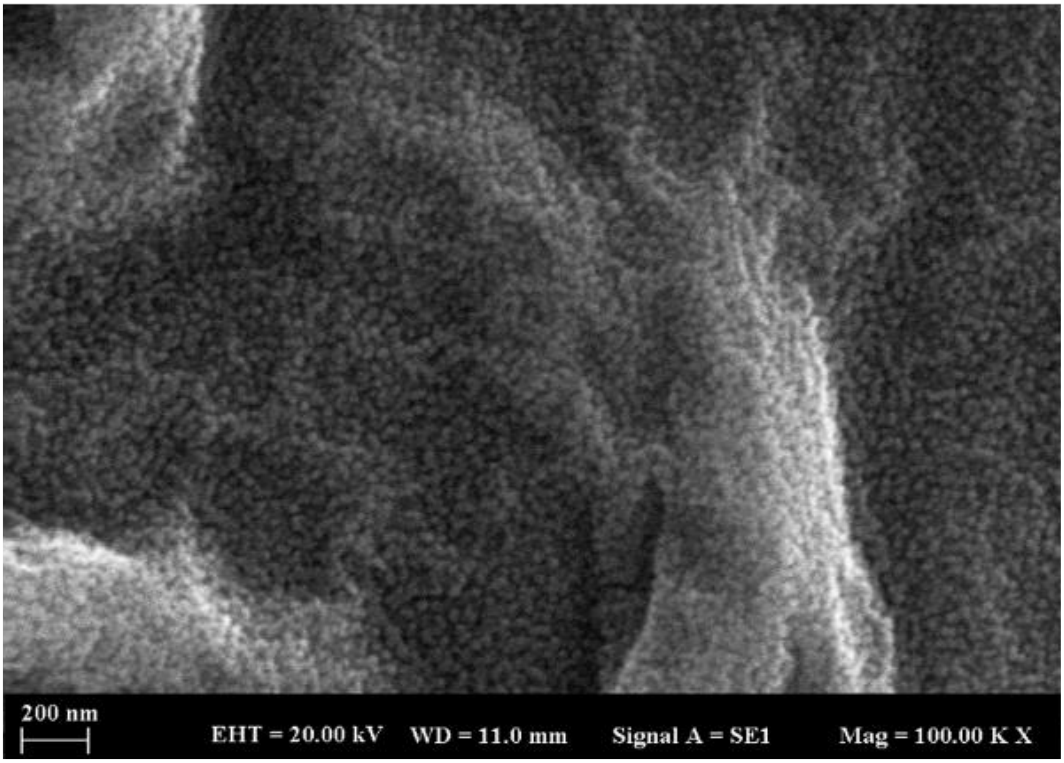

(e)

Fig. 3. SEM image of a) Z, b) C1, c) C2, d)C3 and e) C5 with 100.000 magnification

The chemical compositions of the produced thin films Z, C1, C2, C3, and C5, as well as the ratios of these components in the compound, were determined using the EDS spectra shown from Fig. 4(a) to Fig. 4 (e), respectively. According to the obtained results, the Z thin film is pure ZnO and its compositions exhibit a nearly stoichiometric distribution. Similarly, Co-doped samples contain only Zn, Co, and O elements in their compounds. Although we have produced pure Co-doped ZnO, the ratios of Zn and Co ions within ZnO are lower than their nominal values. The addition of Co elements into ZnO may lead to the formation of defects, such as zinc vacancies and oxygen interstitials, within the crystal structure. Although the amount of Co remains almost constant despite increasing doping rates, suggesting a limit to its solubility within ZnO, it is observed that the physical properties of the ZnO material change as the Co doping rate varies. This situation may be due to the sample not being homogeneous or the presence of defects during sample preparation. In previous studies, it was observed that as the concentration of Co in the initial solution increased, the ratio of its presence in ZnO decreased considerably compared to its nominal value [32, 33]. The situation actually arises from the limited and typically low solubility of cobalt in ZnO. Indeed, particularly low annealing temperatures and the choice of solvents in this study may have restricted the solubility of Co in the ZnO matrix. Simultaneously, this circumstance could have led to a non-uniform distribution of Co within the structure. Moreover, cobalt ions are likely to cause oxidation or reduction reactions on the ZnO surface. This suggests that excess oxygen may cause an acceptor effect and suppress the number of free carriers [34].

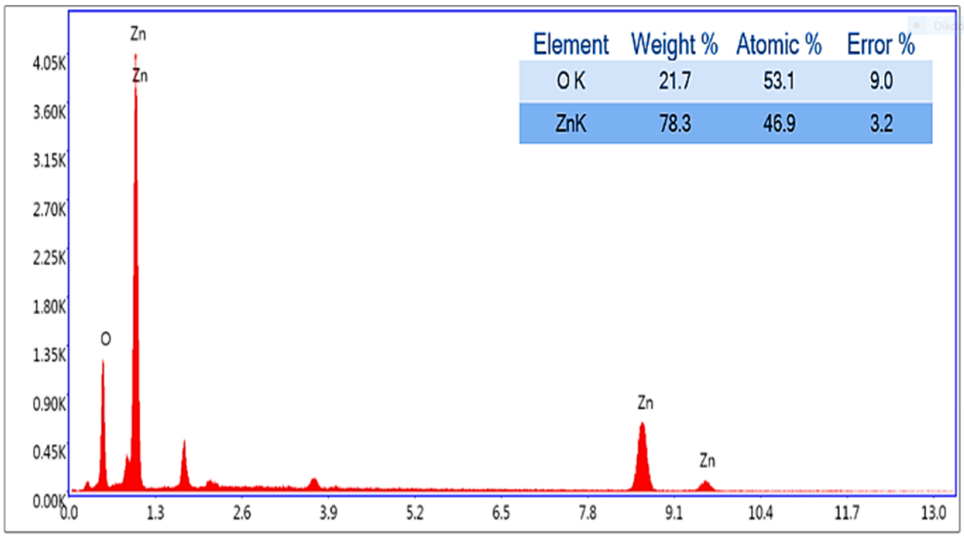

Lsec:30.0 455Cnts 1740 keV Det:Element-C2B

(a)

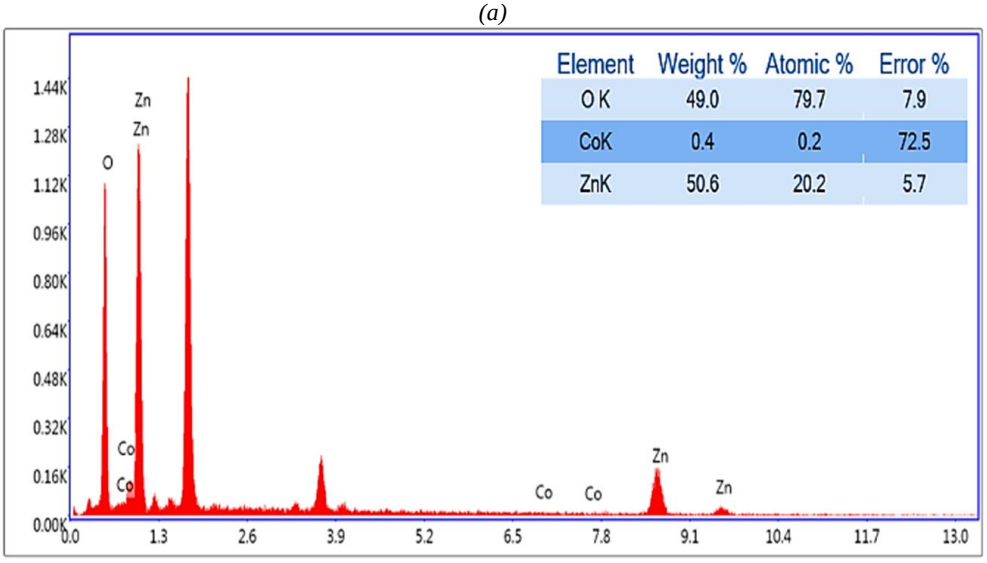

Lsec:30.0 1.442K Cnts 1740 keV Det:Element-C2B

(b)

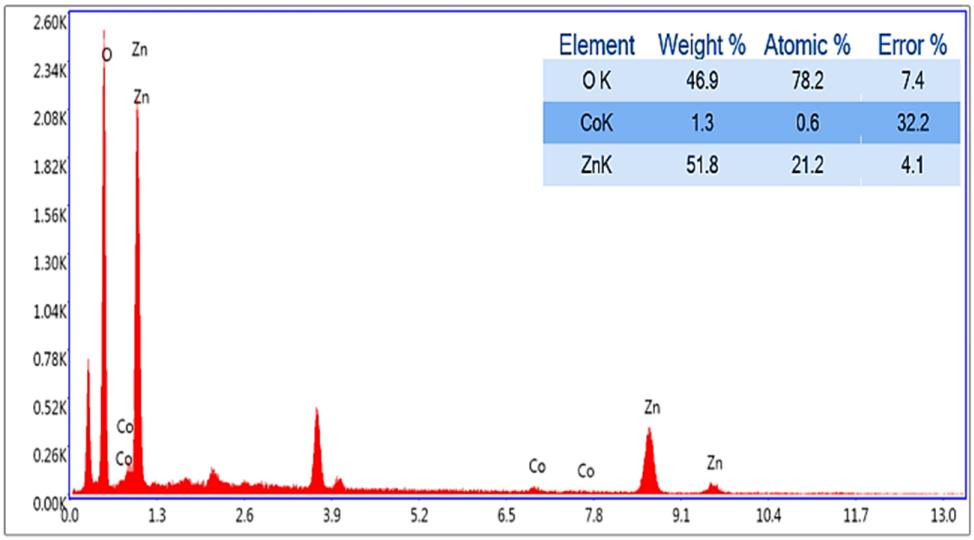

Lsec:30.0 94 Cnts 1740 keV Det:Element-C2B

(c)

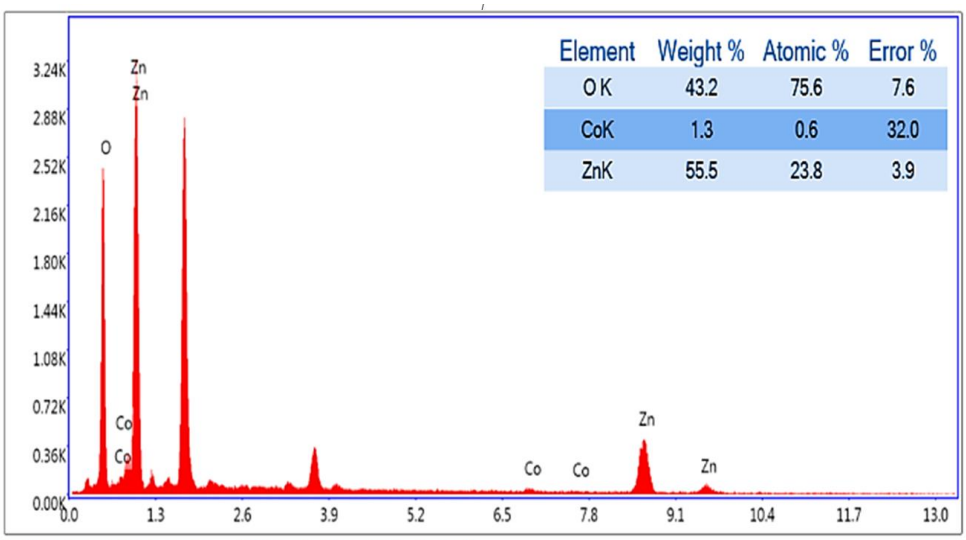

(d)

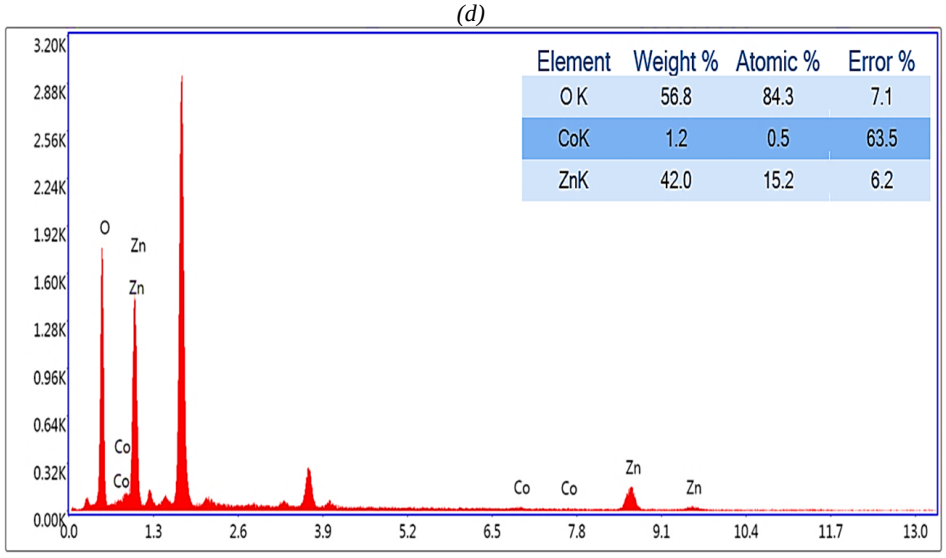

(e)

Fig. 4. EDS spectra of a) Z, b) C1, c) C2, d) C3, and e) C5 samples (color online)

The XRD spectra of $Zn_{1-x}Co_xO$ (x=0.0, 0.01, 0.02, 0.03, and 0.05) thin films on glass substrates are exhibited in Fig. 5. The XRD analysis reveals that all detected peaks indicate the samples are in the form of the wurtzite ZnO polycrystalline structure. It is seen that the dominant crystal orientation for both pristine ZnO and Co-doped ZnO samples is in the (002) plane. An increase in the intensities of the XRD peaks is observed with cobalt doping. This situation indicates that doping enhances the crystal quality of the structures. The best crystal quality is obtained for the C2 thin film. At Co doping values above 2%, the intensities of the XRD peaks start to decrease. Due to this observation, we hypothesize that the solubility limit value in this study may be determined as 6% Co content [34]. This idea is supported by the EDS results. Despite increasing the Co doping ratio, the presence of Co in the compound does not exceed the value of 0.6 for the C2 sample. Additionally, as the doping level increases, a slight leftward shift occurs in the positions of the XRD peaks compared to pristine ZnO. The shift in peaks observed in XRD is influenced by the ionic radii of the dopant. Since the ionic radius of Co^{2+} (58 pm) is smaller than that of Zn^{2+} (60 pm), the strain occurring within the structure or the decrease in the interplanar distance may have caused this situation. Furthermore, for doping ratios of 2% and above, additional peaks corresponding to the (102) and (112) planes appear in the XRD spectrum. As the amount of Co doping increases, this indicates that the samples develop a more polycrystalline structure, and the Co ions form different preferential growth directions. Moreover, the XRD pattern does not exhibit any peak points associated with secondary or impurity phases induced by Co doping.

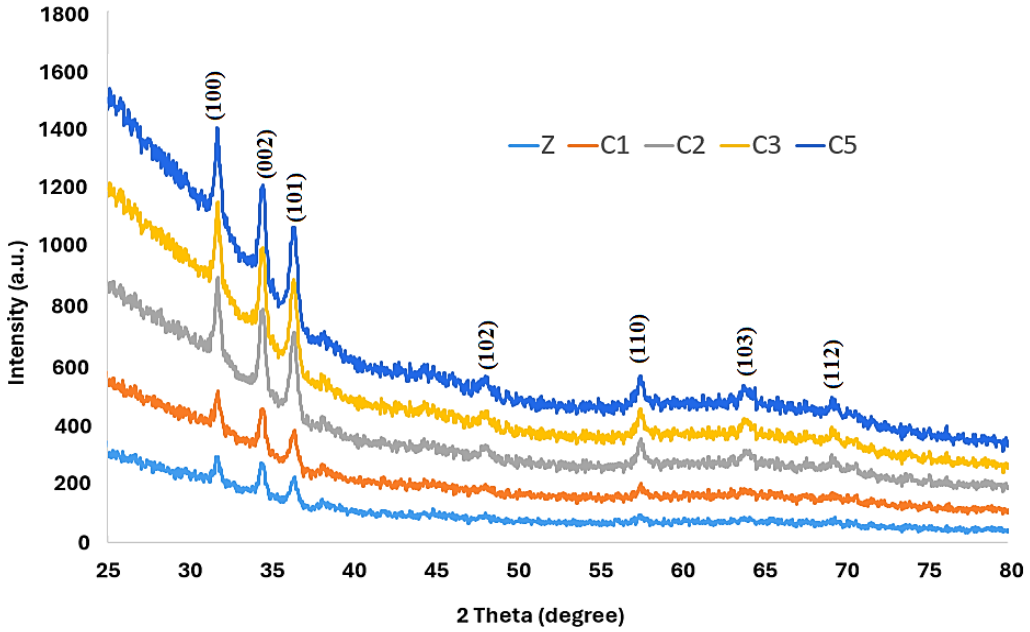

Fig. 5. XRD patterns of produced thin films (color online)

Some parameters related to the crystal structure such as lattice constants (a=b, c for hexagonal unit cell), interplanar distances (d-spacing), crystallite size (D), and microstrain (ε) can be determined using data obtained from XRD spectra. The crystallite size is calculated using the Debye-Scherrer formula, which can be expressed by the following equation [35].

$$D = \frac{0{,}9\,\lambda}{\beta\cos\theta}, \tag{1}$$

where λ is the wavelenght of the X-ray (1,54 Å), β is the FWHM (Full Width at Half Maximum) value of XRD peak, and θ represents the Bragg angle. The distance between crystal planes (d-spacing) is determined using Bragg's law, which is formulated as $d = \lambda/2\sin\theta$. After the interplanar distances were found, lattice parameters of hexagonal crystal structure were calculated with the equation given in Eq. 2 [36].

$$\frac{1}{d^2} = \frac{4}{3}\left(\frac{h^2+hk+k^2}{a^2}\right) + \frac{l^2}{c^2}, \tag{2}$$

where $h, k,$ and l indicate the Miller indices of crystal plane, and d is the interplanar distance. Microstrain is a measure of the internal stresses and deformations within a material. The microstrain formula is given in Eq. 3 [37].

$$\varepsilon = \frac{\beta}{4\tan\theta} \tag{3}$$

All calculated values related to the crystal structure with respect to the (002) plane are presented in Table 1. A decrease in the lattice parameters and interplanar distances of ZnO is observed with cobalt doping. Since Zn and Co ions have similar diameters, there is no significant change in microstrain values for low doping percentages, but it increases significantly for 5% doping.

Table 1. The values of crystal structure parameters for produced thin films

Samples	d (Å)	a (Å)	c (Å)	D (nm)	ε (10^{-3})
Z	2.608	3.199	5.215	25	5.0
C1	2.605	3.197	5.210	29	4.2
C2	2.604	3.196	5.209	23	5.3
C3	2.598	3.188	5.197	25	4.9
C5	2.600	3.190	5.200	14	9.0

The optical properties of both fabricated pristine ZnO and Co-doped ZnO thin films were examined through optical transmittance analysis in this study. The optical transmittance of thin films was measured in the wavelength range of 200-1100 nm at room temperature. The measurement results are shown in Fig. 6 (a). The band gap energy of all thin films (Fig. 6(b)) was determined utilizing these optical transmittance data, employing the Tauc model [38] as described in Eq. 4.

$$(\alpha h\nu) = B\left(h\nu - E_g\right)^{1/2}, \tag{4}$$

where, α, h, ν, and B represent the absorption coefficient, Planck constant, frequency, and a constant related to material, respectively. E_g is the band gap energy of the semiconductor.

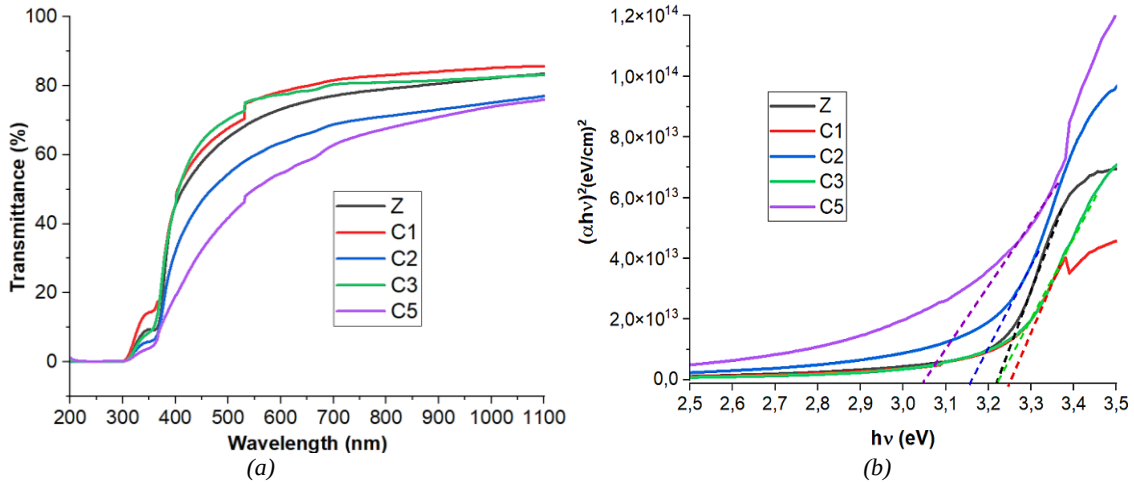

Fig. 6. (a) Optical transmittance of (b) Band gap energies of $Zn_{1-x}Co_xO$ (x=0.0, 0.01, 0.02, 0.03,and 0.05) samples (color online)

The values obtained from these graphs for optical transmittance and band gap energies are presented in Table 2.

Table 2. Optical properties of all samples

Sample	Average optical transmittance (%)	Average band gap energy (eV)
Z	70	3.22
C1	75	3.25
C2	60	3.16
C3	75	3.22
C5	55	3.05

Among all the produced samples, only the 1% Co-doped ZnO sample exhibited increased optical transmittance in the visible region and band gap energy compared to pristine ZnO. Cobalt doping can influence the concentration and mobility of charge carriers (electrons and holes) in ZnO. At low doping concentrations, the introduction of cobalt ions may increase the concentration of charge carriers, leading to a band gap widening due to increased screening effects [39]. However, the decrease in the band gap observed in the other samples, except for C3, can be attributed to various factors. Furthermore, this decrease can primarily be attributed to the sp-d exchange interaction occurring between the localized d electrons and the band electrons of the Co ions integrated into the ZnO lattice [40]. Another reason for the decrease in the band gap could be the shallow type defect levels formed within the structure due to Co doping. Particularly, it is evident from the EDS analysis results that Zn vacancies are formed within the structure. These zinc vacancies can create shallow acceptor type defect levels above the valence band. Additionally, donor energy levels may form just below the conduction band due to Co doping. All of these shallow type defect and donor levels could have contributed to the reduction in the band gap. The band gaps of the Z and C3 thin films are found to be identical. However, apart from the band gaps of these two samples, the results regarding their crystal structure are also similar. If cobalt ions primarily substitute zinc ions in the ZnO lattice (substitutional doping), the structural and optical properties of the material may not be drastically altered. Substitutional doping at low concentrations may preserve the crystal structure and optical characteristics of ZnO, resulting in similar properties. Additionally, the relatively low doping ratio may have contributed to this result. The XRD analysis reveals similar microstrain conditions for Z and C3 sample. In fact, this indicates that the atomic arrangements in the lattice and the resulting defects are similar in the two samples. Moreover, the Co dopants could have induced compensating defects that counteract the changes in the band structure. Moreover, if the Co dopants are segregated at grain boundaries or interfaces, their influence on the overall band gap could be limited.

Optical transmittance measurements were used not only to determine the optical properties of the samples but also to estimate thin film thicknesses. The Swanepoel method was employed to determine the thicknesses of all films, relying on optical transmittance graphs. Detailed information about the Swanepoel method can be found in Reference [41]. The approximate thicknesses of Z, C1, C2, C3, and C5 thin films are obtained as 380 nm, 430 nm, 620 nm, 570 nm, and 675 nm, respectively. It is clearly seen that the optical transmittances of the samples in the visible region vary depending on the thickness and decrease as the thickness increases. The undoped ZnO thin film is transparent, whereas Co-doped ZnO thin films exhibit decreased optical transmittance with a deepening green color as the concentration of Co increases [34].

I–V characteristics of the Au/$Zn_{1-x}Co_xO$ (x=0.0, 0.01, 0.02, 0.03, and 0.05)/p-type Si MIS (metal/interlayer/semiconductor) structures under the dark environment are depicted in Fig. 7 for the voltage range between -3V and 3V. In linearly scaled I-V measurements, particularly under forward bias, it is observed that pure ZnO exhibits significantly higher current compared to doped ZnO thin films. This actually indicates that the conductivity of Z is better than that of other samples (Fig. 7(a)). Negative differential resistance (NDR) is clearly observed for the Z sample in Fig. 7 (a). This phenomenon in undoped ZnO may be attributed to tunneling current

between the Au contact and the material [42]. Moreover, the decrease in current after reaching a certain voltage value can be related to high serial resistance [43]. In the C5 sample, it is observed that the current value under forward bias is quite close to the leakage current. Consequently, a decrease in the current magnitude is observed under forward bias regions as the doping level increases. The decline in film conductivity can be attributed to the improvement in crystalline quality, as evidenced by the XRD results. The presence of Co atoms occupying interstitial positions introduces crystal defects, effectively acting as scattering centers. The electrical conductivity values are closely linked to the grain size, where smaller grains enhance grain boundary scattering mechanisms [34]. Consequently, in this study, it is observed that grain boundary scattering increases with decreasing grain size, particularly for higher Co content samples. Another reason is the presence of excess oxygen, which creates an acceptor effect in the structure, in Co-doped samples, especially in the C5. The average leakage current (I_0) of all thin films is determined by identifying the point where the linear line of the forward voltage region intersects the y-axis in the semi-logarithmic I-V graph (Fig. 7 (b)). It is observed that the average leakage current of each doped ZnO samples is smaller than that of pristine ZnO. Particularly, a noticeable decrease in leakage current is noticed with increasing doping ratios. This situation may have resulted in a decrease in average leakage current due to the acceptor type defect levels, such as zinc vacancies or oxygen interstitials, formed within the lattice through cobalt doping. According to the EDS results, the sample with the highest zinc vacancies in the structure is determined as C5. Additionally, the average resistances of the samples are idenfied from the I-V graphs. The obtained results are listed in Table 3. In addition to the formation of defects with doping, XRD and SEM analyses indicate that the decrease in crystal size will increase grain boundary scattering, or excess oxygen leading to a noticeable increase in resistance, particularly in the C5 sample. In parallel, there is a significant decrease in electrical conductivity for C5 sample compared to pristine ZnO.

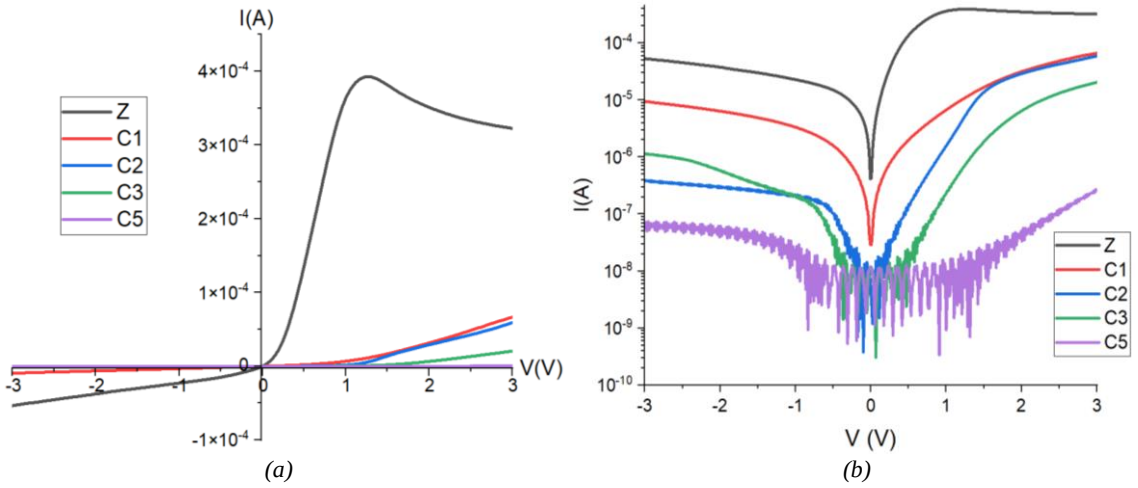

Fig. 7. Dark I-V characteristic of undoped ZnO and Co-doped ZnO with different Co moles with a)linear scale, b)semi-logaritmic scale (color online)

Table 3. Average leakage current and resistance of undoped ZnO and Co-doped ZnO samples

Samples	Average I_0 (A)	Average R (Ω)
Z	1.9×10^{-6}	2.3×10^{4}
C1	1.0×10^{-6}	3.3×10^{4}
C2	3.4×10^{-8}	3.8×10^{4}
C3	1.0×10^{-8}	7.5×10^{4}
C5	3.8×10^{-9}	4.0×10^{6}

The gradual decline in fossil resources for energy production is heightening interest in renewable energy sources. Among these, the sun emerges as the most abundant, clean, environmentally friendly, and readily available option. Solar cells harness sunlight to generate electricity, making them a focal point of intensive research efforts. A solar cell is characterized by open circuit voltage (V_{OC}), short circuit current (I_{SC}), fill factor (FF), and efficiency (η). The open-circuit voltage is the voltage at which the current in the I-V characteristic of a solar cell, operating under sunlight, is zero, while the short-circuit current is the current when the voltage is zero. The fill factor is calculated as the ratio of the maximum power (P_M=I_M xV_M) obtained from the I-V graph to the product of open circuit voltage and short circuit current. Efficiency (η) of the solar cell is expressed as the product of open circuit voltage, short circuit current, and fill factor divided by the power of the incident light on the solar cell (P_{in}). This relationship is formulated as $\eta = \frac{V_{OC} I_{SC} FF}{P_{in}}$ [44].

Cobalt-doped with different mole ratios and undoped ZnO thin films, coated on p-type Si substrates, were analyzed for their optoelectronic properties, including solar cell and photodiode characteristics under illumination with the power of 100 mW/cm². The J-V (current density-voltage) graphs, which allow us to find

the parameters related to the solar cell, are presented in Figs. 8 (a) and (b) only for Z and C1 thin films, respectively. Notably, the photovoltaic cell efficiency in Co-doped ZnO coated films with additive ratios of 2% and above (C2, C3, and C5 thin films) is nearly zero; hence, graphs and values of these samples are not illustrated in this study.

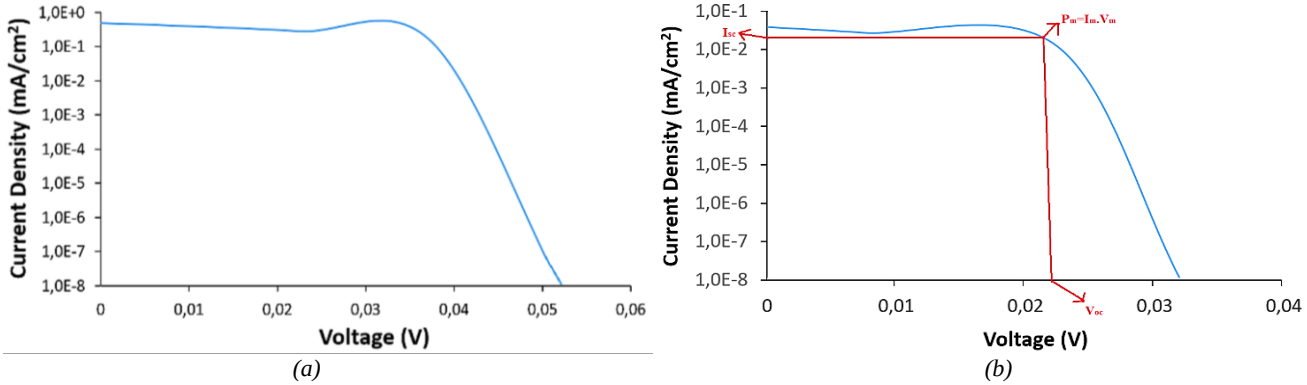

(a) *(b)*

Fig. 8. Current density–voltage (J–V) curves of solar cells for a) undoped ZnO, b) 1% Co doped ZnO (color online)

The open circuit voltage, short circuit current, fill factor, shunt resistance (R_{SH}), and solar cell efficiency of Z and C1 thin films are provided in Table 4.

Table 4. The solar cell paremeters and their values of Z and C1 samples

Samples	J_{SC}(mA/cm^2)	V_{OC}(V)	FF	η(%)	R_{SH}(Ω.cm^2)
Z	$4.7x10^{-1}$	~$5.2x10^{-2}$	0.26	~ $7.0x10^{-3}$	2.6
C1	$3.7x10^{-2}$	~$3.2x10^{-2}$	~ 0.27	$3.0x10^{-4}$	5.5

The results indicate that the undoped ZnO thin film outperforms others as a solar cell. In all examples, low short-circuit currents and open-circuit voltages indicate very low shunt resistances. It is established that low shunt resistance diminishes both open circuit voltage and short circuit current [45]. The pores formed during coating can indeed decrease the shunt resistance by creating short circuits within the structure via metal contact. However, the metal contacts can also contribute to an increase in series resistance, particularly when using Au as contact materials. In addition to these factors, deep type defect levels formed by doping may also have reduced the solar cell performance of the samples. All results obtained for solar cells indicate that the addition of cobalt to ZnO is not suitable for solar cell applications.

In today's rapidly evolving technological landscape, optoelectronic devices have become indispensable tools, revolutionizing the way we interact with and harness light. These devices, which bridge the realms of optics and electronics, hold immense significance across various fields, from communications and energy to sensing and imaging. Photodiodes, among optoelectronic devices, hold significant technological importance. They convert light energy into electrical signals, finding applications in information, data transmission, sensing systems, image sensors, optical communications, and various other fields [46]. Therefore, the photodiode properties of all samples were investigated in the study. In photodiodes, the sensitivity of diodes under feedback to light is examined. In standard diodes, a small leakage current is expected to occur under reverse voltage, typically ranging from nano to microamperes. However, when photodiodes are exposed to light, this leakage current undergoes a significant increase. Fig. 9 illustrates the variation of leakage current for each thin film under reverse bias in both dark and illuminated conditions. Furthermore, Fig. 9 also depicts the current variation in the forward bias regions under both dark and illuminated conditions.

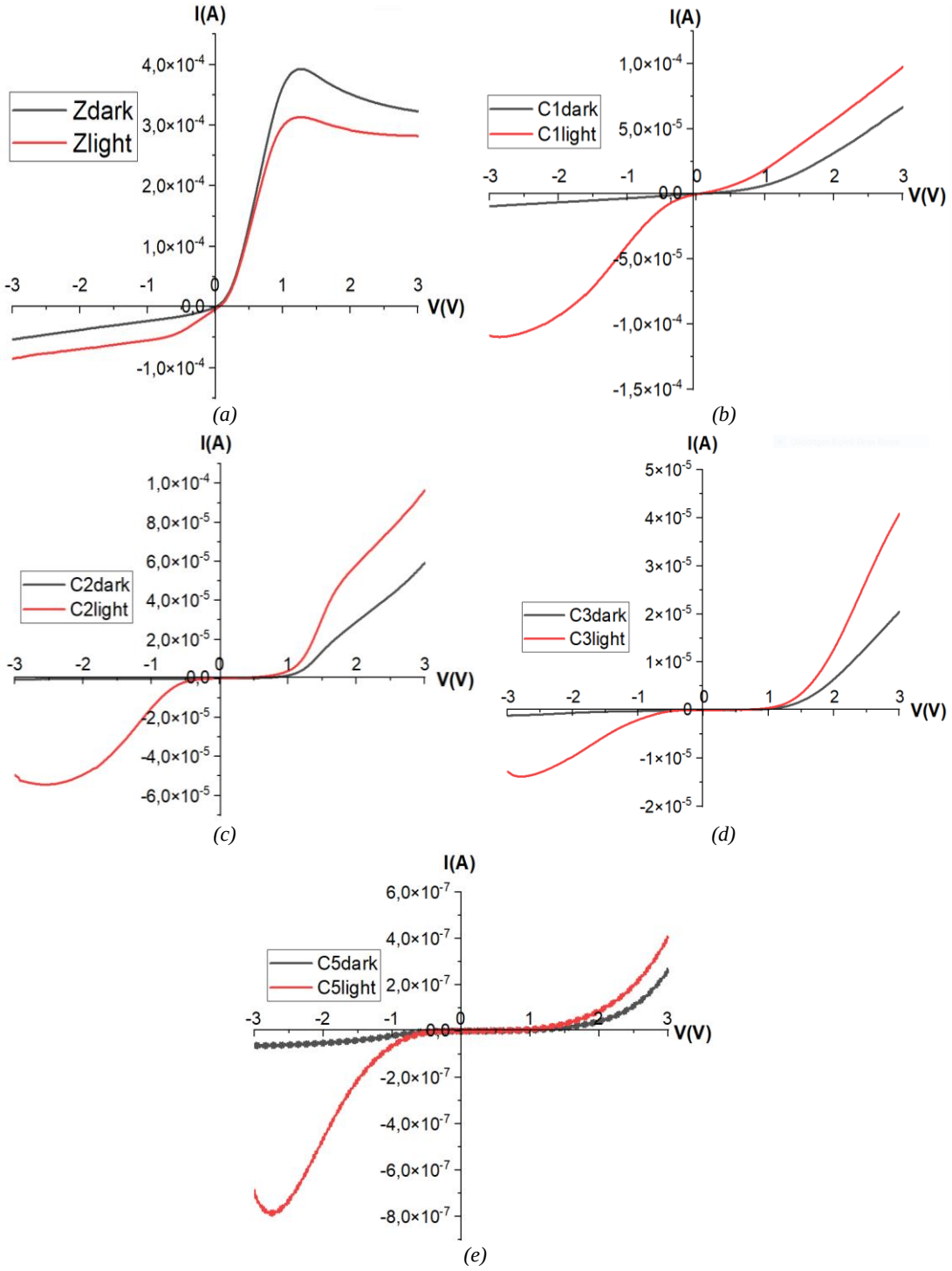

Fig. 9. Photodiode properties of (a) Z, (b) C1, (c) C2, (d) C3, and (e) C5 samples (color online)

It is evident from Fig. 9 that C1 exhibits the most favorable photodiode properties for visible light among the fabricated thin films. In fact, it can be inferred that the performance of nearly all cobalt-doped samples in this study surpasses that of pristine ZnO as photodiode. The increase in leakage currents of Co-doped samples with illumination in the visible region can be attributed to deep acceptor type defect levels. The presence of deep type defect levels may also explain the low solar cell and electrical performance of doped thin films. It is proposed that the Zn vacancy is a dominant acceptor type defect in ZnO, which is consistent with the findings reported by Tuomisto et al. [47]. They were observed two energy levels of the Zn vacancy above the valence band at 0.7 and 2.4 eV. The obtained results in this study may be related to defect levels above 2.4 eV from the valence band [48]. Furthermore, the presence of Zn vacancies is supported by EDS results. However, the decrease in band gap can also be attributed to the formation of lower energy Zn vacancies in the system. As the Co doping concentration

increases, a decrease in leakage current under illumination in the feedback region is observed. This situation could actually be an indication of the more intense formation of shallow acceptor type defect levels rather than deep type defect levels. This is consistent with the band gap energies of doped samples as well.

Photoresponsivity typically refers to the ability of an optoelectronic device, usually a photodetector, to respond to light of a specific wavelength, essentially evaluating its capability to convert the amount of detected light into electrical signals. Photoresponsivity (R) can be expressed using Eq. (5) [49].

$$R = \frac{I_p - I_d}{P_{in}}, \quad (5)$$

where I_p represents the current generated under illumination, I_d is the leakage current in the dark, and P_{in} is the power of the incident light (100 mW/cm^2) on the sample. The photoresponsivity values of thin films at various Co doping ratios are depicted in Fig. 10 for a reverse bias of 3 V. The photoresponsivity of the 1% Co-doped ZnO/p-type Si diode is 1.27x10^{-1} AW^{-1}, while it is 4x10^{-2} AW^{-1} for undoped ZnO. The obtained value for C1 sample represents the best result among all samples. Moreover, its response to the visible light spectrum is remarkable. Conversely, the worst result is observed for C5 sample, with a value of 8.0x10^{-4} AW^{-1}.

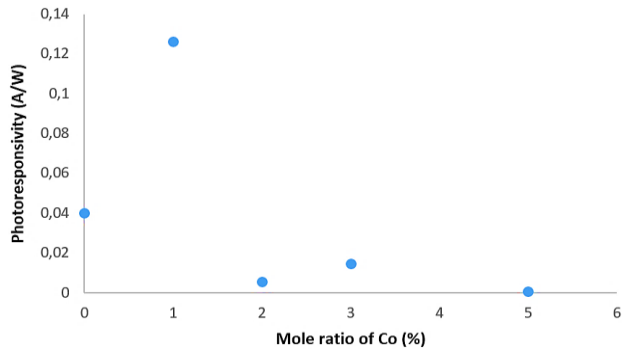

Fig. 10. Photoresponsivity values of all diodes according to their Co doping ratios (color online)

Finally, Fig. 11 displays the phototransient current plots of all diodes, including undoped ZnO and Co-doped ZnO diodes.

When samples are illuminated with light in the visible region, a decrease in current is observed in pristine ZnO, while an increase in current is observed in all Co-doped samples. It is well-known that ZnO is an effective UV photodetector, which could explain its insensitivity to visible light. Pure ZnO has a wide band gap, typically around 3.3 eV, which means it absorbs mostly UV light. Under visible light illumination, which has lower energy compared to UV light, ZnO absorbs fewer photons due to its band gap absorption characteristics. As a result, the generation of electron-hole pairs is reduced, leading to a decrease in phototransient current. The Co-doped ZnO diodes, especially those with 1% Co doping, demonstrate favorable photoconductivity behavior. Upon turning off the light, the current attributed to photons in the Co-doped ZnO samples experienced a sudden decrease. The response of doped samples to visible light may be attributed to defects or the density of surface states induced by doping. Addionationaly, the lack of response of pristine ZnO to visible light may be attributed to its typically lacking carrier levels formed at deep defect levels that could respond to the visible spectrum.

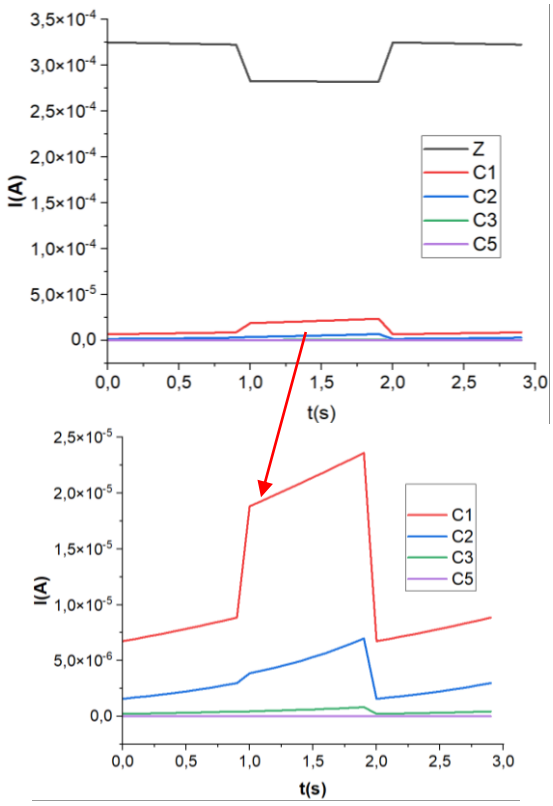

Fig. 11. Phototransient current plots of all diodes (color online)

In summary, based on the aforementioned results, it has been concluded that cobalt is not a suitable dopant element for solar cells. Furthermore, it can be inferred that the performance of pure ZnO is significantly enhanced in terms of structural, and photodiode properties with 1% Co doping.

4. Conclusions

$Zn_{1-x}Co_xO$ (x= 0.0, 0.01, 0.02, 0.03, and 0.05) thin films were fabricated on glass and p-type Si substrates using the sol-gel dip coating and spraying method. Structural analysis revealed that all thin films were pure and exhibited the wurtzite ZnO polycrystalline structure with the preferred orientation along the (002) plane. Despite their purity, deviations from the stoichiometric ratio of Zn, Co, and O elements were anticipated, potentially leading to point defects within the structure. Particularly, the doped samples displayed nanofiber surface morphologies composed of nanodots. It was

observed that the surface homogeneity of the thin films improved with Co doping, and the most favorable outcome observed in the 1% Co-doped ZnO sample (C1 sample). Additionally, the crystal size of ZnO decreased with doping. The crystal size of pure ZnO, which was 25 nm, decreased to 14 nm with 5% cobalt doping (C5 sample). As the amount of doping increased, the microstrain of the structure also increased from 5.0×10^{-3} to 9.0×10^{-3}, depending on film thickness and defects formed in the thin films. At low cobalt doping ratios, no significant changes were observed in the optical transmittance and band gap energy of ZnO due to smiliar ionic radii of Zn and Co elements. However, with higher doping amount (5% Co doping), a decrease in optical transmittance from 70% to 55% and a reduction in the band gap energy from 3.22 eV to 3.05 eV were observed. This phenomenon can be attributed to increased film thickness with higher effective defect densities and sp-d exchange interaction. According to the I-V measurements taken under dark conditions, pristine ZnO exhibited low resistance and high leakage current values compared to doped samples. As the dopant ratio increased, the resistance of the samples increased, and the leakage currents decreased. While a significant change was not observed for low doping rates, the resistance value of ZnO thin film increased from $2.3\text{x}10^{4}$ Ω to $4.0\text{x}10^{6}$ Ω for 5% Co doping, accompanied by a decrease in leakage current from $1.9\text{x}10^{-6}$ A to $3.8\text{x}10^{-9}$ A. The significant decrease in current in high cobalt-doped thin films in the forward bias region is also remarkable. This situation can be attributed more to the decrease in particle size, leading to increased grain boundary scattering, or to the formation of deep defect levels or excess oxygen within the film. When examining the optoelectronic properties of Au/$Zn_{1-x}Co_xO$/p-type Si diodes, particularly as solar cells and photodiodes, it is evident that the efficiency of Co-doped ZnO thin films as solar cells is very low. This is likely attributed to the presence of very low shunt resistance or deep type defect levels observed in the samples. Consequently, Co dopant material is deemed unsuitable for usage in solar cells. However, comparatively good results are achieved with various Co-doped ZnO samples, notably the 1% Co-doped sample (C1), when used as photodiodes, particularly for the visible region. The highest photoresponsivity is observed in the C1 sample, reaching $1.27\text{x}10^{-1}$ AW^{-1}.

Although Co doping improved the optical and structural properties of ZnO, decreases in electrical and solar cell efficiencies were observed. Although we believe that the most important factor negatively affecting the solar cell and electrical efficiency of thin films is the Co dopant element, it would be incorrect to say that it is the only parameter. Additionally, the pores and non-homogeneous film structure created by the spraying method, which allows one-sided film coating for these measurements, may have been influential. However, due to defect levels formed within the structure, particularly for 1% Co-doped ZnO, favorable results were achieved as a photodiode against visible light. Therefore, ZnO doped with 1% Co may be a promising material in the field of optoelectronics as a photodiode. In summary, the study results indicate that Co doping yielded the most favorable outcomes at around 1%, with no significant positive effects observed, especially in instrumental applications, for doping levels exceeding this rate.

Acknowledgements

This study was financially supported by the Research Fund of the Istanbul University (Project number FYL-2021-37947) and TÜBİTAK with project number 121F465 in Turkey. The authors would like to thank Abdullah Ateş, head of I.U. Strategy Department and Associate Professor Cemil Akçay from Architecture Faculty of Istanbul University for their support. Also, the author would like to thanks Associate Professor Barış Kınacı from Photonics Application and Research Center, Gazi University for his unmatched assistance in taking electrical measurements.

References

[1] L. P. Peng, L. Fanga, X. F. Yang, Y. J. Li, Q. L. Huang, F. Wu, C. Y. Kong, J. Alloys Compd. **484**, 575 (2009).
[2] J. Yang, X. Liu, L. Yang, Y. Wang, Y. Zhang, J. Lang, M. Gao, M. Wei, J. Alloys Compd. **485**, 743 (2009).
[3] F. Yakuphanoğlu, J. Alloys Compd. **494**, 451 (2010).
[4] S. Liang, H. Sheng, Y. Liu, Z. Huo, Y. Lu, H. Shen, J. Cryst. Growth **225**,110 (2001).
[5] W. T. Yen, Y. C. Lin, J. H. Ke, Appl. Surf. Sci. **257**, 960 (2010).
[6] A. Mahroug, S. Boudjadar, S. Hamrit, L. Guerbous, Materials Letters **134**, 248 (2014).
[7] Y. Peng, D. Jiang, M. Zhao, Y. Duan, H. Wei, H. Li, Q. Liang, S. Wang, J. Alloys Compd. **965**, 171372 (2023).
[8] K. Tang, M. Jiang, B. Yang, T. Xu, Z. Liu, P. Wan, C. Kan, D. Shi, Nanoscale **15**, 2292 (2023).
[9] S. Thambidurai, P. Gowthaman, M. Venkatachalam, S. Suresh, M. Kandasamy, J. Alloys Compd. **852**, 156997 (2021).
[10] G. Dong, J. Li, Y. Zhao, X. Ran, C. W. Peng, D. He, C. Jin, Q. Wang, H. Jiang, Y. Zhang, X. Cao, C. Yu, Progress in Photovoltaics: Research and Applications **31**, 9 (2023).
[11] Z. Chen, J. Wang, H. Wu, J. Yang, Y. Wang, J. Zhang, Q. Bao, M. Wang, Z. Ma, W. Tress, Z. Tang, Nat. Commun. **13**, 4387 (2022).
[12] A. C. Badgujar, B. S. Yadav, G. K. Jha, S. R. Dhage, ACS Omega **7(16)**, 14203 (2022).
[13] D. Zhang, W. Yu, L. Zhang, X. Hao, Materials **16**, 5537 (2023).
[14] S. Vinoth, A. M. S. Arulanantham, S. Saravanakumar, R. S. R. Isaac, N. Soundaram, N. Chidhambaram, D. Alagarasan, S. Varadharajaperumal, M. Shkir, S. AlFaify, J. Mater. Sci.: Mater. Electron **32**, 27060 (2021).
[15] Y. Zhang, L. Wu, H. Li, J. Xu, L. Han, B. Wang,

Z. Tuo, E. Xie, J. Alloys Compd. **473**, 319 (2009).
[16] Y. Lin, D. M. Jiang, F. Lin, W. Z. Shi, X. M. Ma, J. Alloys Compd. **436**, 30 (2007).
[17] S. K. Neogia, R. Ghoshb, G. K. Paulb, S. K. Berac, S. Bandyopadhyay, J. Alloys Compd. **487**, 269 (2009).
[18] L. H. Van, M. H. Hong, J. Ding, J. Alloy. Compd. **449**, 207 (2008).
[19] A. Kaphle, P. Hari, Thin Solid Films **657**, 76 (2018).
[20] F. Bouhjar, L. Derbali, B. Marí, Nano Res. **13**, 2546 (2020).
[21] G. Kanimozhi, S. Vinoth, H. Kumar, E. S. Srinadhu, N. Satyanarayana, Mater. Res. Express **6,** 025041 (2019).
[22] A. Kaphle, P. Hari, Thin Solid Films **657**, 76 (2018)
[23] H. S. Al-Salman, M. J. Abdullah, J. Mater. Sci. Technol. **29(12)**, 1 (2013).
[24] A. N. Ech Chergui, C. Pflitsch, B. Atakan, Surf. Interfaces **22**, 100883 (2021).
[25] M. Stachowicz, J. M. Sajkowski, M. A. Pietrzyk, D. Nd. Faye, S. Magalhaes, E. Alves, A. Reszka, A. Pieniążek, A. Kozanecki, Thin Solid Films **781**, 140003 (2023).
[26] E. H. Ahmed, M. A. Ahmed, M. M. Sabri, J. Opt. **53**, 712 (2024).
[27] G. M. Mirza, M. M. H. Tusher, N. Sakib, M. N. Islam, J. Mater. Sci.: Mater. Electron. **34**, 1542 (2023).
[28] L. Arab, A. Amri, A. Meftah, A. Latif, T. Tibermacine, N. Sengouga, Chem. Phys. Impact **7**, 100266 (2023).
[29] B. Houng, C. J. Huang, Surface and Coatings Technology **201**, 3188 (2006).
[30] Ö. Çelik, Ş Baturay, Y. S. Ocak, Mater. Res. Express **7**, 026403 (2020).
[31] B. Unveroglu Abdioglu, Physica B **684**, 415968 (2024).
[32] Dhruvashi, P. K. Shishodia, Thin Solid Films **612**, 55 (2016).
[33] P. Li, S. Wang, J. Li, Y. Wei, Journal of Luminescence **132**, 220 (2012).
[34] O. Gençyilmaz, F. Atay, İ. Akyüz, Journal of Nanoelectronics and Optoelectronics **10**, 1 (2015).
[35] P. Scherrer, Nachr. Ges. Wiss. Göttingen **26**, 98 (1918).
[36] N. Üzar, Appl. Phys. **124**, 303 (2018).
[37] D. W. Fu, W. Zhang, H. L. Cai, J. Z. Ge, Y. Zhang, R. G. Xiong, Adv Mater. **23**, 5658 (2011).
[38] J. Tauc, Amorphous and Liquid Semiconductors Plenum, Springer, 159 (1974).
[39] M. Kaur, V. Kumar, J. Singh, J. Datt, R. Sharma, Materials Technology **37(13)**, 2644 (2022).
[40] T. Thangeeswari, A. T. George, A. Arun Kumar, Indian Journal of Science and Technology **9(1)**, 1 (2016).
[41] D. Dorranian, L. Dejam, G. Mosayebian, J. Theor. Appl. Phys. **6**, 13 (2012).
[42] D. Sang, J. Liu, X. Wang, D. Zhang, F. Ke, H. Hu, W. Wang, B. Zhang, H. Li, B. Liu, Q. Wang, Front. Chem. **8**, 531 (2020).
[43] A. Rahmati, M. Yousefi, Zeitschrift für anorganische und allgemeine Chemie **643**(1), 870 (2017).
[44] https://www.pveducation.org/pvcdrom/solar-cell-operation/solar-cell-efficiency
[45] M. Kamran, Fundamentals of Smart Grid Systems, Academic Press, 219 (2023).
[46] T. Para, Optoelectronics-Recent Advances, IntechOpen, United Kingdom, 150 (2023).
[47] F. Tuomisto, V. Ranki, K. Saarinen, D. C. Look, Phys. Rev. Lett. **91**, 205502 (2003).
[48] F. Oba, M. Choi, A. Togo, I. Tanaka, Sci. Technol. Adv. Mater. **12**, 034302 (2011).
[49] Z. N. Ng, Y. Chan, Journal of Physics: Conference Series **1349**, 012043 (2019).

*Corresponding author: neslihanuzar@istanbul.edu.tr